Responses of bistable piezoelectric-composite energy harvester by means of recurrences

Arkadiusz Syta[1], Christopher R. Bowen[2], H. Alicia Kim[3], Andrzej Rysak[1], Grzegorz Litak[1] *

[1]*Faculty of Mechanical Engineering, Lublin University of Technology, Nadbystrzycka 36, PL-20-618 Lublin, Poland*
[2]*Department of Mechanical Engineering, University of Bath, Bath, BA2 7AY, United Kingdom*
[3]*Structural Engineering, Jacobs School of Engineering, University of California San Diego, 9500 Gilman Drive, La Jolla, CA 92093, US.*

Abstract

In this paper we examine the modal response of a bistable electro-mechanical energy harvesting device based on characterisation of the experimental time-series. A piezoelectric element attached to a vibrating bistable carbon-fibre reinforced polymer laminate plate was used for the conversion of mechanical vibrations to electrical energy under harmonic excitations at a variety of frequencies and amplitudes. The inherent bistability of the mechanical resonator and snap-through phenomenon between stable states were exploited for energy harvesting. To identify the dynamics of the response of the studied harvesting structure and the associated output power generation we used the Fourier spectrum and Recurrence Quantification Analysis (RQA).

keywords: energy harvesting, piezoelectric, snap-through, non-linear vibrations, recurrence plots

Number of figures: 8
Total number of pages in the manuscript: 15

Submitted to *Mechanical Systems and Signal Processing*

*Corresponding author: Email: g.litak@pollub.pl Tel: +48 695132143, Fax: +48 815384233

1 Introduction

Due to the increasing use of wireless sensor networks and growth in the demand for electronics requiring a portable energy source, energy harvesting devices have been developed in an attempt to convert ambient mechanical vibrations into electrical energy. The transduction mechanism employed for vibration harvesting include electrostatic generation, electromagnetic induction, and the piezoelectric effect. Piezoelectric based composite laminates have been studied extensively in recent years for application as a potential piezoelectric energy harvesting system [1]. In the present work we study a bistable electromechanical system based on a piezoelectric fibre composite device coupled to a carbon fibre reinforced polymer (CFRP) laminate. The CFRP laminate has an asymmetric layup, $[0/90]_T$, so that it exhibits bistability and under the application of sufficiently large mechanical vibrations it can undergo snap-through between its two stable states to generate electrical energy by the direct piezoelectric effect [2, 3]. The use of bistability is of interest since it has been shown to improve the broadband response of the harvesting device [4]. The use of smart materials, such as piezoelectric materials, for energy harvesting applications range from battery-free pace-makers [5] to structural health monitoring of civil or aerospace structures [1, 6, 7, 8]. Detailed reviews of the literature on energy harvesting from vibration have been given by Sodano et al. [9], Anton and Sodano [10], Cook-Chennault et al. [11] and Priya and Inman [13]. Furthermore, Pellegrini et al. [12] and Harne and Wang [14] have recently presented focused reviews on the topic of nonlinear vibration energy harvesting. Piezoelectric and ferroelectric materials and structures for energy harvesting applications were also reviewed by Bowen et. al. [15]. The present paper identifies a nonlinear mechanical resonator response leading to effective energy harvesting by using an asymmetric CFRP laminate plate with a piezoelectric patch attached to the structure. The present paper presents investigations on a nonlinear mechanical resonator response to understand the complex system dynamics and improve energy harvesting with piezoelectics.

2 The experimental set-up

A square $[0/90]_T$ laminate was considered as the basis for developing a broadband energy harvesting device. The laminate measured 190mm x 190 mm and was made from M21/T800 CFRP prepreg material. A single piezoelectric Macro Fiber Composite (MFC) layer (M8585-P2, 85 x 85 mm) was attached to the laminate surface by adhesive bonding. This particular piezoelectric device is polarized through the thickness of the piezoelectric fibres so that the direct d_{31} piezoelectric effect (charge per unit force) is aligned with the major curvature of the dominant shape. Such a device configuration also exhibits a high capacitance (typically 800 nF) compared to piezoelectric devices polarized along their length, leading to lower voltage outputs. Additional masses in the form of steel bolts (12 g each) were attached to the four corners of the laminate to increase the achievable curvatures and aid snap-through during oscillation using a mechanical shaker (see Fig. 1).

The device was mounted to an electro-dynamic shaker (LDS V455) and a 15 mm circular section carefully removed from the MFC-laminate combination to allow attach-

(a)

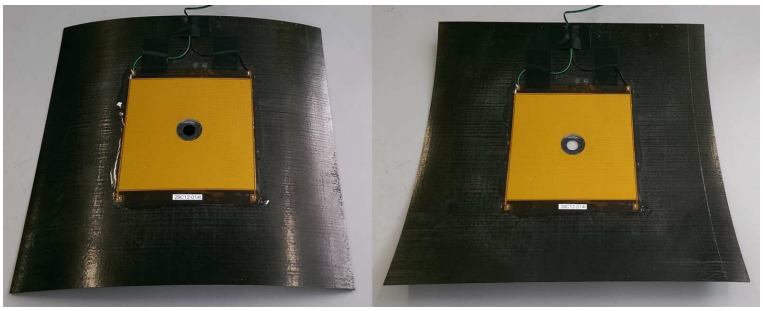

(b)

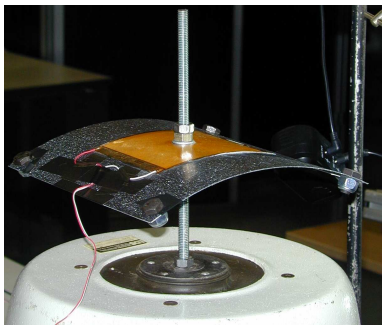

Figure 1: (a) Stable shapes of a $[0/90]_T$ piezoelectric plate, and (b) experimental setup showing mechanical shaker attachment. The sampling time step was 0.00024 s (4230 Hz).

ment to the shaker system. The MFC positive and negative electrodes were attached to an oscilloscope (Agilent 54835A) to measure the open-circuit voltage outputs that were developed during testing. A range of vibration frequencies and amplitudes were applied using the shaker to characterize the harvester and the dynamic response. The laminate displacement was monitored via a Digital Image Correlation (DIC) system [2]. For further studies we selected the displacement due to bending of the plate at one of corners.

The examples of measured displacement data are presented in Fig. 2. Note even in the short intervals it is possible to notice different dynamic response which is mainly caused by different bending shapes. Identification of the particular response would be the central point of our discussion in the present note. A visual inspection confirmed that Fig. 2a corresponds to a single well (small amplitude without snap-through) oscillations, while Fig. 2b-d exhibit snap-through. Interestingly, these complex snap-though system responses exhibit chaotic (non-periodic), periodic with intermittent snap-throughs, and repeatable behaviour.

In the Tab. I, we summarize the system conditions (input amplitude and frequency) and measured response averages (standard deviation of the corner displacement and root mean square (RMS) of voltage output for the open circuit measurements. Note that we used the frequencies close to the resonance where the nonlinear effects are most pronounced. The efficiency, measured by a ratio RMS of voltage output voltage to RMS of displacement input, shows that the case of repeatible snap-through (d) is the best for energy harvesting while chaotic snap-through (b) is better than intermittent snap-through (c). Finally, the single well case (a) is characterized by the smallest efficiency. The average

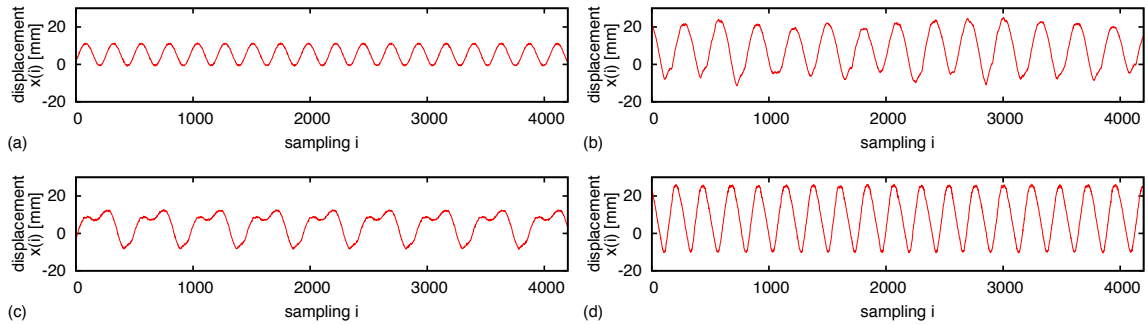

Figure 2: Magnitude of corner displacement for (a) low amplitude oscillations (20.8 Hz, 6 mm peak-to-peak displacement), (b) chaotic snap-through (20.8 Hz, 7 mm), (c) intermittent snap-through (20.8 Hz, 9 mm), and (d) repeatable snap-through (18 Hz, 3.5 mm).

voltage output indicates that energy harvesting is the most efficient in the case (d) while is the worst in the case (a). It is also clear that the case (b) is better for energy harvesting comparing to (c) as the amplitude of central point excitations is smaller in (b).

Table 1: Statistics of the representative experimental results (time series).

Case	frequency [Hz]	input amplitude of the center point displacement [mm]	standard deviation of the corner mass displacement x [mm]	RMS of the voltage output u [V]	Efficiency RMS(u)/RMS(x) [V/mm]
(a)	20.8	6	4.30	2.12	0.50
(b)	20.8	7	11.11	14.10	2.85
(c)	20.8	9	6.46	13.84	2.17
(d)	18	3.5	13.22	14.86	6.00

The corresponding Fourier spectra are presented in Fig. 3. Note that the experimental data are very short in terms of the excitation cycles (Fig. 2). Therefore, point-to-point measurement noise component plays an important role in the frequency spectrum. Note that, in case of a non-periodic system response (Fig. 3b) the visible peaks in the Fourier spectra are quenched and broadened compared to similar amplitude regular-like response in Fig 3c-d (intermittent snap-through and repeatable snap-through, respectively). Note also the difference in scales in all the cases. After more careful inspection, one can notice that the case (b) is characterized by a heavier tail of the decay trend with increasing frequencies while the cases (a) and (c) show smaller main peaks. Interestingly, the single peak visible in the case (a) is splitted into two in (b). Such a splitting indicate the bifurcation from single well to snap-through vibrations.

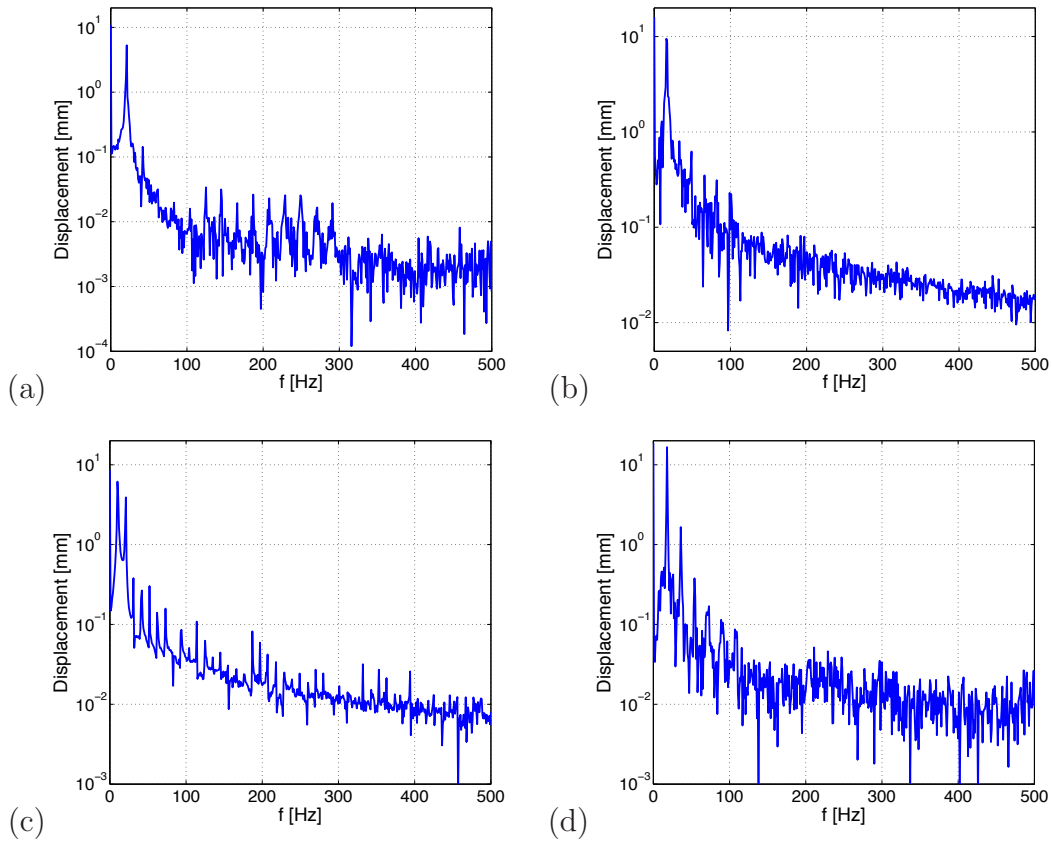

Figure 3: Fourier spectra in a logarithmic scale. Fig. 3(a)-(d) cases correspond to Fig. 2 (a)-(d). Note different scales in vertical axes.

3 Reconstruction of phase space

Given scalar observation $y(t)$ of length n it is possible to reconstruct a smooth attractor in m dimensional space:

$$\mathbf{y} = [y(t), y(t-\tau), y(t-2\tau), ..., y(t-(m-1)\tau)]\,, \tag{1}$$

where τ is time delay, m is embedding dimension [18, 21, 20, 19]. Generally speaking, any time delay can be assumed, but choosing too small value of τ causes vectors in the reconstructed phase space to be strongly correlated. On the other hand, choosing a τ value that is too large leads to weak correlations between the vectors and the information about detailed dynamics in a short period of time can be lost. One of the methods for choosing an appropriate time delay is the average Mutual Information function (MI) [22] which takes into account nonlinear dependencies of data.

Namely,

$$MI = -\sum_{ij} p_{ij}(\tau) \log \frac{p_{ij}(\tau)}{p_i p_j}, \tag{2}$$

where for some partition on the real numbers p_i is the probability to find a time series value in the i-th interval, and $p_{ij}(\tau)$ is the joint probability that an observation falls into the i-th interval and the observation time τ later falls into the j-th (the observation range is divided into 16 intervals). In this context the time delay τ is chosen as a first minimum of MI (Fig. 4(a)). Thus the time delay for each case (a)-(d) (see cases in Figs. 2 and 3 and the corresponding minima of MI in Fig. 4(a) was $\tau = \{12, 88, 39, 10\}$, respectively.

The estimated time delay τ is used as an input to calculate the embedding dimension m by the method of fraction of False Nearest Neighbours, FNN, [21, 20, 19]

Assuming the m-dimensional Euclidean space, the examined time series can be represented by the position vector $\mathbf{y}_i$ where i corresponds to the discrete sampling time (see Eq. 1). Considering each point $\mathbf{y}_i$ and its nearest neighbour $\mathbf{y}_j$, one can calculate the distance $||\mathbf{y}_j - \mathbf{y}_i||_m$. By iterating both points and comparing the ratio

$$R_{im} = \frac{||\mathbf{y}_j - \mathbf{y}_i||_{m+1}}{||\mathbf{y}_j - \mathbf{y}_i||_m} \tag{3}$$

to the threshold R_t (here $R_t = 2$) one increases the number of false neighbours if $R_{im} > R_t$ for the given dimension m. Its fraction with respect to the total number of considered points defines FNN.

This can be simply done by increasing the dimension and viewing the reconstructed attractor until false crossing of trajectories vanish. A more systematic approach is to use the false nearest neighbour fraction function that increases the dimension until the number of FNN reduces to zero (Fig. 4(b)).

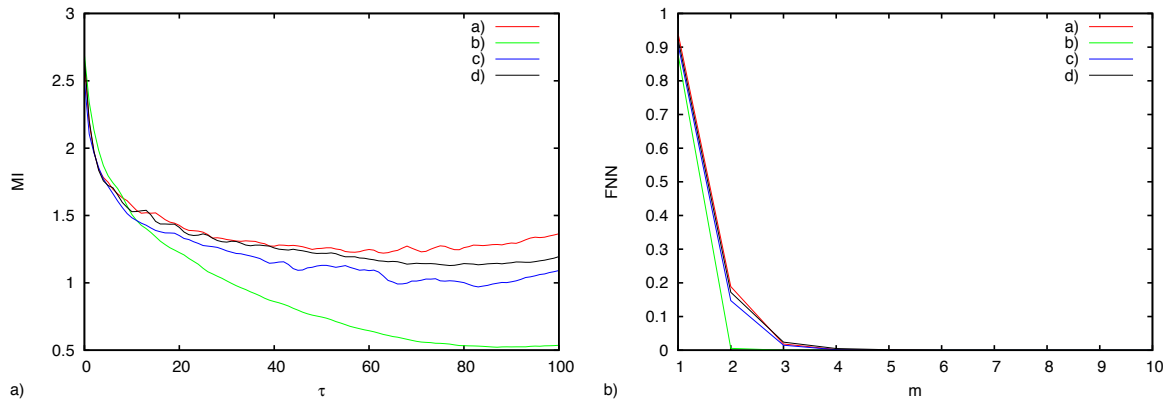

Figure 4: (a) Average mutual information MI versus time delay τ, (b) fraction of false nearest neighbours FNN, versus embedding dimension m.

When comparing the embedding dimension in Fig. 4(b) one can see it is lower for chaotic case ($m = 3$) while it approaches the same value for the other cases ($m = 4$). Nevertheless, we choose the largest dimension $m = 4$ for subsequent analyses because in higher dimensions the false crossings of trajectories vanish. Figure 5 shows projections of reconstructed phase space onto three dimensions. On analysing phase portraits Fig. 5, different vibration patterns of the harvesters are broadly characterised into three groups: (i) oscillations which remain in a single well state (Fig. 4(a) , (ii) those which undergo

motion between two stable states in chaotic patterns (Fig. 4(b)), (iii) those which undergo motion between two stable states in an intermittent but periodic pattern (Fig. 4(c)) and (iv) those which travel repeatedly between the two stable states at each vibration cycle (Fig. 4(d)).

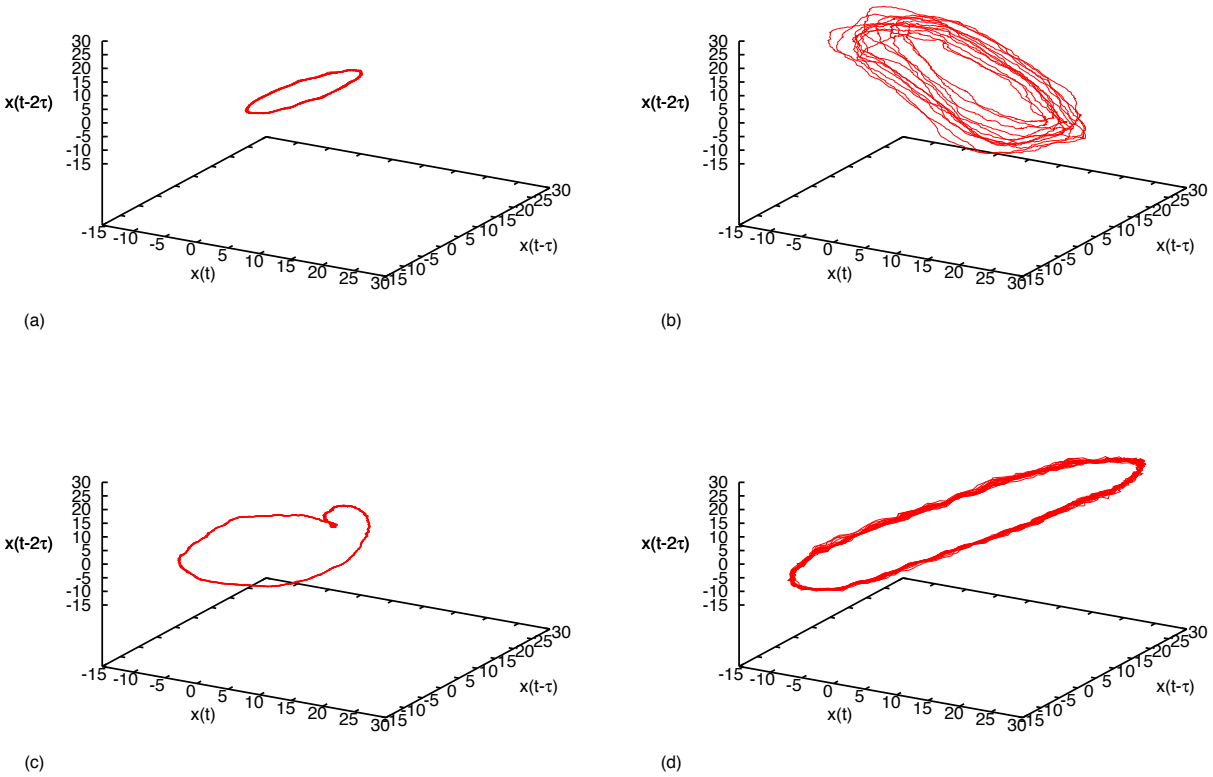

Figure 5: Reconstructed attractors for the consecutive subplots are numbered as in Figs. 2 and 3. (a) low amplitude oscillations (20.8 Hz-forcing frequency, 6 mm peak- to-peak displacement), (b) chaotic snap-through (20.8 Hz, 7 mm), (c) intermittent snap-through (20.8 Hz, 9 mm), and (d) repeatable snap-through (18 Hz, 3.5 mm).

4 Recurrence Quantification Analysis

The periodicity of the underlying dynamics can be investigated by means of recurrences which is calculated for each point of the reconstructed trajectory. This method was developed by Eckmann [23] and extended by Webber [24], Casdagli [28] later by Marwan et al. [25, 29] and others. This method can be applied for both short deterministic and noise experimental data ([31, 30]). Two points on a trajectory are marked as neighbours if they are close enough to each other and this can be expressed by the distance matrix

R with its element R^{ϵ}_{ij} given by [23]:

$$R^{\epsilon}_{ij} = \Theta(\epsilon - ||\mathbf{x}_i - \mathbf{x}_j||), \tag{4}$$

where ϵ is the threshold value and $\Theta(x)$ denotes the Heaviside function. The number of recurrence points depends on both the underlying dynamics and the threshold value. A standard technique for approximations is that the threshold value should not be higher than a few percentage of the total number of points [29]. Figure 6 compares recurrence plots (RP) of 2% of recurrence points calculated with Euclidean distance in the reconstructed phase space. The horizontal and vertical axes represent the time instants i and j for which the distance formula (Eq. 4) is applied.

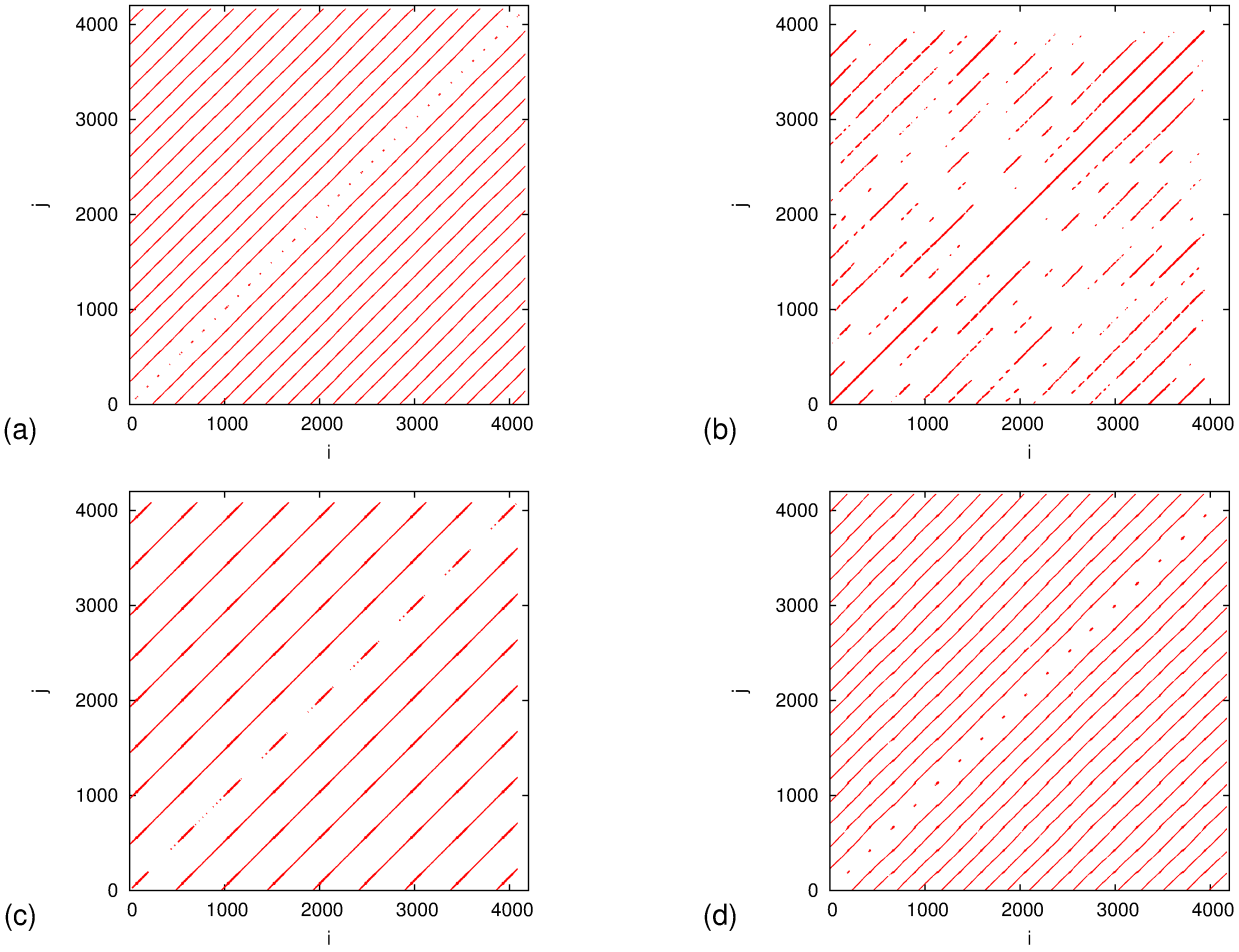

Figure 6: Recurrence plots of the corner displacement with same number of points $RR = 0.02$ (Eq. 5). for all cases: (a)-(d) denoted as in Figs. 2(a)-(d) and Tab. I, respectively. Note that the identity center diagonal $i = j$ is excluded.

The periodic nature of the system is visible by the diagonal lines on the recurrence plot (Fig. 6 a,c and d) while the nonperiodic (chaotic) behaviour exhibits short diagonal lines with isolated points (Fig. 6b). Note that the main diagonal representing the nodal

distance of the same states and is excluded from the RPs.

An additional method can be used to compare the dynamics of the system for different center point displacement excitation by recurrences and calculating the distance matrix for the same threshold value. Figure 7 shows the RP obtained for normalized (by the standard deviation) displacement and the same value $\epsilon = 0.1$ for each case.

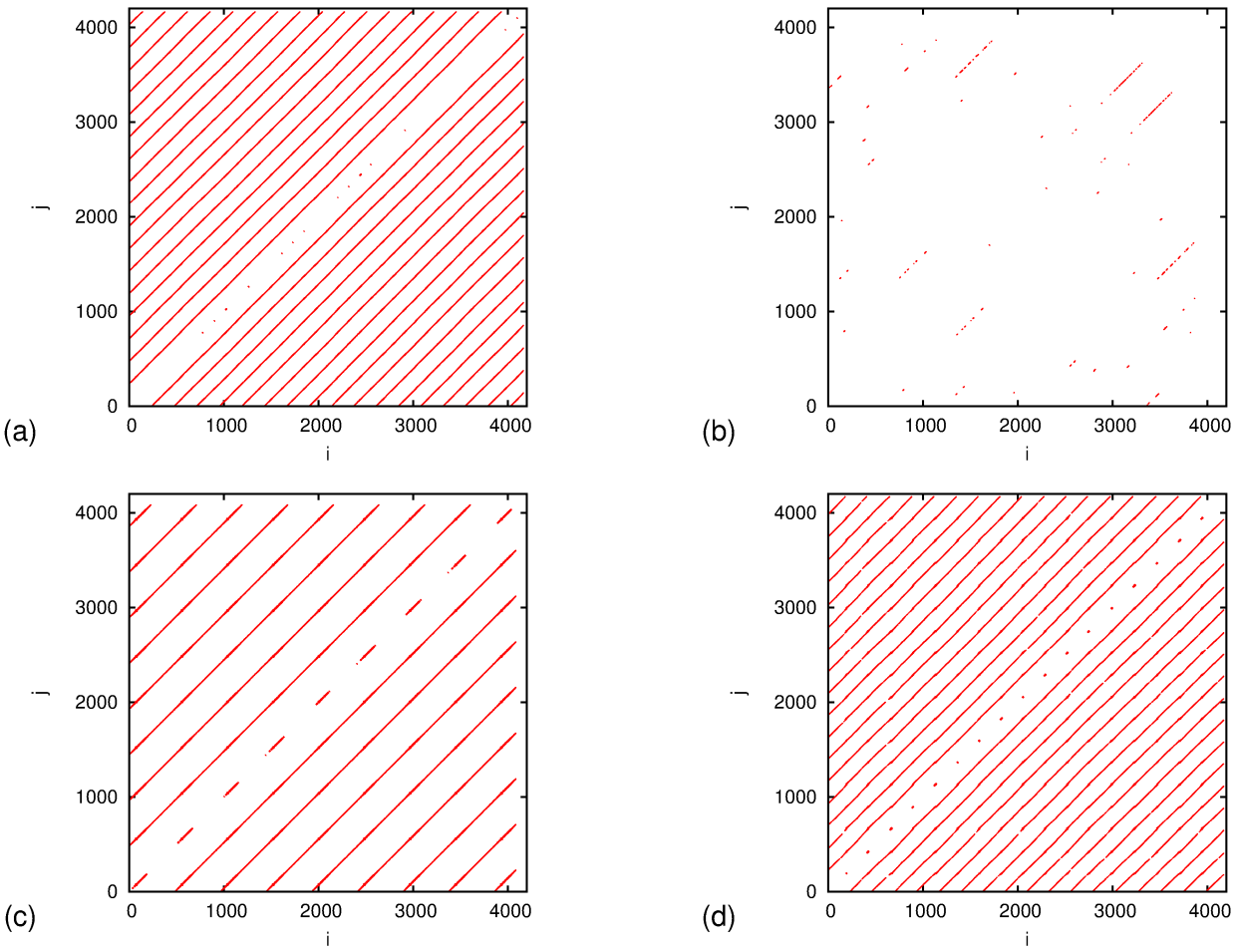

Figure 7: Recurrence plots of normalized displacement for all cases: (a)-(d) denoted as in Figs. 2(a)-(d) and Tab. I, respectively, for $\epsilon = 0.1$. Note that the identity center diagonal $i = j$ is excluded.

In this case it is clearly visible that the RP of the chaotic case contains less points than the periodic ones which indicates a lack of periodicity. The diagonal lines are much shorter indicating short intervals of states recurrences (or periodicity with given tolerance ϵ).

Webber and Zbilut [24] and later Marwan et al. [25, 29] developed the Recurrence Quantification Analysis (RQA) for recurrence plots. The RQA analysis includes the recurrence rate variable, RR, which is a measure of ability for the system to return to the

neighbourhood of previous state and has the following definition,

$$RR = \frac{1}{N^2} \sum_{i,j \neq i}^{N} R_{ij}^{\epsilon}. \tag{5}$$

Furthermore, the RQA can be used to identify diagonal and vertical lines through their maximal lengths $LMAX$, $VMAX$ for diagonal and vertical lines, respectively. The RQA provides the probability $p(l)$ or $p(v)$ of line distribution according to their lengths l or v (for diagonal and vertical lines). They are calculated as

$$p(z) = \frac{P^{\epsilon}(z)}{\sum_{x=x_{min}}^{N} P^{\epsilon}(z)}, \tag{6}$$

where $z = l$ or v depending on diagonal or vertical structures in the specific recurrence plot. $P^{\epsilon}(z)$ denotes the histogram of z lengths and a fixed value of ϵ.

Measures such as: determinism DET, laminarity LAM, trapping time TT and average length L, are based on probabilities $P^{\epsilon}(z)$

$$DET = \frac{\sum_{l=l_{min}}^{N} l P^{\epsilon}(l)}{\sum_{l=1}^{N} l P^{\epsilon}(l)}, \tag{7}$$

$$LAM = \frac{\sum_{v=v_{min}}^{N} v P^{\epsilon}(v)}{\sum_{v=1}^{N} v P^{\epsilon}(v)}, \tag{8}$$

$$L = \frac{\sum_{l=l_{min}}^{N} l P^{\epsilon}(l)}{\sum_{l=l_{min}}^{N} P^{\epsilon}(l)}, \tag{9}$$

$$TT = \frac{\sum_{v=v_{min}}^{N} v P^{\epsilon}(v)}{\sum_{v=v_{min}}^{N} P^{\epsilon}(v)}, \tag{10}$$

where l_{min} and v_{min} denote minimal values which should be chosen for a specific dynamical system (here $l_{min} = v_{min} = 2$). The determinism DET is a measure of the predictability of the examined dynamical system and provides the ratio of the recurrence points formed in diagonals to all recurrent points. Note that in a periodic system all recurrence points would be included in the lines parallel to the main diagonal. On the other hand, the laminarity LAM is a similar measure which corresponds to points formed in vertical lines. This measure indicates the dynamics behind sampling point changes. For small (slow) point-to-point changes the consecutive points form a vertical line. Finally, the average diagonal length L refers to the predictability time of a dynamic system while the trapping time TT indicates the average length of the vertical lines measuring the time scale (in terms of sampling intervals) of small changes in the examined time history. Note that by introducing the above statistical definitions (Eqs. 5-10) it is possible to parametrize any RP of the physical data by using the meaningful parameters as determinism, laminarity, trapping time, etc.

More insights into the system dynamics can be provided through calculating recurrence variables for diagonal and vertical lines. They are presented in Tables II and III.

Values of RQA statistics in Tab. II (for fixed RR value) do not settle between periodic and non-periodic character of the corner displacement of the harvester resonator. First of all, the DET values are at the same high level which indicates a low influence of noise.

Table 2: Recurrence analysis based on diagonal and vertical lines for various cases. For each case $RR = 0.02$.

case	ϵ	DET	$LMAX$	L	LAM	$VMAX$	TT
a	0.5	0.950	626	17.7	0.995	15	5.3
b	3.8	0.987	3931	26.1	0.996	27	11.3
c	0.9	0.975	3601	19.9	0.954	27	10.2
d	1.6	0.956	282	10.5	0.988	22	5.0

Table 3: Recurrence analysis based on diagonal and vertical lines for various cases. For each case $\epsilon = 0.1$.

case	RR	DET	$LMAX$	L	LAM	$VMAX$	TT
a	0.015	0.940	544	13.9	0.991	10	4.1
b	0.001	0.913	23	5.8	0.921	7	3.1
c	0.014	0.965	3601	14.9	0.992	21	7.2
d	0.014	0.930	169	7.3	0.963	19	3.8

The longest diagonal line is received for the chaotic case (b) and slightly lower for the periodic case (c). This is surprising as the diagonal line structures are responsible for the periodical motion. However the longest line visible in Fig. 6b is the next to the central diagonal for fairly larger ϵ. Moreover the diagonal structure for the periodic case has a repeatable structure of equidistant lines (Fig. 6c).

A supporting chaotic behaviour argument can be found in the values of laminarity which is minimal for case (b).

A clearer distinction between the types of the vibrations can be found in Tab. III (for fixed ϵ). One can observe minimal values (slightly lower) of determinism, laminarity and mean diagonal obtained for the non-periodic (chaotic) case. Additionally, distinctly shorter maximal length of the diagonal line (23) obtained for case (b) reflects a lower predictability of the system.

Therefore, it can be said that the fixed small ϵ assumption provides a possibility of distinguishing between periodic and the chaotic responses of a excited bistable plate for a reasonably short time series. Moreover the differences in L, $LMAX$, $VMAX$, and TT in Tab. III indicate that snap-through motions can be distinguished from single well vibration.

Figure 8(a) shows the recurrence rate parameter RR while Fig. 8(b) illustrates $LMAX$ versus ϵ.

Figure 8(a) also shows that the chaotic case (curve 'b' in Fig.8a) can be easily distinguished from any other cases by power law ϵ^{α}, where $\alpha > 1$ is a constant exponent, comparing to linear case ($\alpha = 1$) in regular (periodic) vibrations.

On the other hand Fig. 8(b) identifies the snap-through (for a small threshold value: $\epsilon < 0.3$). Clearly, for the single well vibration case (b) $LMAX$ is rising rapidly with ϵ

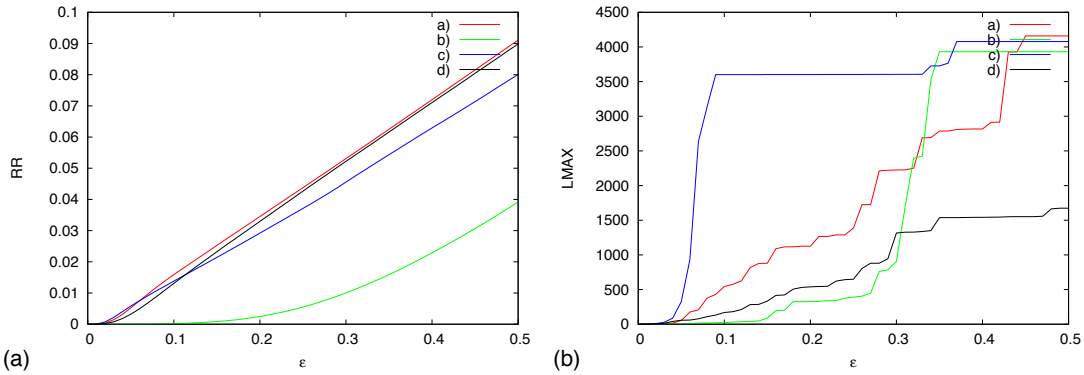

Figure 8: Recurrence rate RR and longest diagonal line $LMAX$ as a functions of threshold ϵ, calculated for all cases (a)-(d) denoted as in Fig. 2 and Tab. I, respectively.

relative to the slower increases when snap-throughs are involved (b),(c), and (d).

5 Conclusions

We have applied the non-linear times series analysis methods based on recurrences in reconstructed phase space to experimental data consisting of dynamics of a bistable piezoelectric-composite energy harvester. We propose RQA analysis to identify the periodic and chaotic responses from fairly short time series. Examination of Figs. 6 and 7 indicates it is clear that one can also consider quantification and identification of different kinds of snap-through motions as was proposed in [31] for the parametric pendulum but more systematic studies should be done. It is worth noting that analysing short time series data is difficult and full of pitfalls. One of them is the influence of measurement and dynamic noise. This was not a concern in this paper as it needs treatments of longer time series data.

Interestingly, the chaotic vibrations of the resonator (see Tab. I) in terms of energy harvesting was found to be more efficient compared to other snap-through responses. 6. This effect is a consequence of nonlinearities. Note that close to the resonance we expect to find resonant (repeatable snap-through) and nonresonat (intermittent snap-through) solutions, while the chaotic solution indicates the intermediate nature with intermediate efficiency. To tell more about it the harvesting efficiency should be studied more systematically to reveal the situation in the resonance region which could be characterized by multiple solutions for given excitation conditions. The system response identification from the relatively short time series may appear to be important for improvement of energy harvesting from bistable plates vibrations.

Acknowledgement

The authors gratefully acknowledge the support of the Polish National Science Center (A.S., A.R., and G.L.) under Grant No. 2012/05/B/ ST8/ 00080.

Bowen acknowledges funding from the European Research Council under the European Union's Seventh Framework Programme (FP/2007-2013) / ERC Grant Agreement no. 320963 on Novel Energy Materials, Engineering Science and Integrated Systems (NEMESIS). Kim acknowledges financial support from the Engineering and Physical Science Research Council (EPSRC) for Project Reference: EP/J014389/1 "Optimisation of Broadband Energy Harvesters Using Bistable Composites".

References

[1] S. Priya, Advances in energy harvesting using low profile piezoelectric transducers, J. Electroceram. 19, 165-182 (2007).

[2] D.N. Betts, C.R. Bowen, H.A. Kim, N. Gathercole1, C.T. Clarke, D.J. Inman, Nonlinear dynamics of a bistable piezoelectriccomposite energy harvester for broadband application, Eur. Phys. J. Special Topics 222, 15531562 (2013).

[3] M. Borowiec, A. Rysak, D.H. Betts, C.R. Bowen, H.A. Kim, G. Litak, Complex response of the bistable laminated plate: Multiscale entropy analysis, European Physical Journal Plus 129, 211 (2014).

[4] A.F. Arrieta, P. Hagedorn, A. Erturk, and D. J. Inman, A piezoelectric bistable plate for nonlinear broadband energy harvesting, Appl. Phys. Lett., 97, 104102 (2010).

[5] M. A. Karami and D. J. Inman, Powering pacemakers from heartbeat vibrations using linear and nonlinear energy harvesters, Appl. Phys. Lett. 100, 042901 (2012).

[6] S. P. Beeby, M. J. Tudor, and N. M. White, Energy harvesting vibration sources for microsystems applications, Meas. Sci. Technol. 17(12), R175R195 (2006).

[7] E. Lefeuvre, A. Badel, A. Benayad, L. Lebrun, C. Richard, and D. Guyomar, A comparison between several approaches of piezoelectric energy harvesting, J. Phys. IV (France) 128, 177186 (2005).

[8] M. Friswell, S. Ali, O. Bilgen, S. Adhikari, A. Lees, and G. Litak, Nonlinear piezoelectric vibration energy harvesting from a vertical cantilever beam with tip mass, J. Intell. Mater. Syst. Struct. 23(11), 15051521 (2012).

[9] H. Sodano, D. Inman, and G. Park, A review of power harvesting from vibration using piezoelectric materials, Shock Vib. Digest 36, 197-205 (2004).

[10] S. R. Anton and H. A. Sodano, A review of power harvesting using piezoelectric materials (2003-2006), Smart Mater. Struct.16, R1-R21 (2007).

[11] K. Cook-Chennault, N. Thambi, and A. Sastry, Topical review: Powering mems portable devices- a review of non-regenerative and regenerative power supply systems with special emphasis on piezoelectric energy harvesting systems, Smart Mater. Struct. 17, 043001 (2008).

[12] S. P. Pellegrini, N. Tolou, M. Schenk, and J. L. Herder, Bistable vibration energy harvesters: A review, J. Intell. Mater. Syst. Struct. 24(11), 1303-1312 (2013).

[13] S. Priya and D. Inman, Energy Harvesting Technologies (Springer, Berlin, Heidelberg, New York, (2008).

[14] R. L. Harne and K. W. Wang, A review of the recent research on vibration energy harvesting via bistable systems, Smart Mater. Struct. 22, 023001 (2013).

[15] C. R. Bowen, H. A. Kim, P. M. Weaver and S. Dunn, Piezoelectric and ferroelectric materials and structures for energy harvesting applications, Energy & Environmental Sci. 7 25-44 (2014).

[16] G. Litak, M. Wiercigroch, B.W. Horton, X. Xu, Transient chaotic behaviour versus periodic motion of a parametric pendulum by recurrence plots, Zeit. Angew. Math. Mech. 90, 33-41 (2010).

[17] A. Syta, J. Jonak, L. Jedlinski, G. Litak, Failure diagnosis of a gear box by recurrences J. Vibr. Acoust. Trans. ASME 134, 041006, (2012).

[18] F. Takens, Detecting Strange Attractors in Turbulence, Lecture Notes in Mathematics, Vol. 898 (Springer, Heidelberg 1981) 366–381.

[19] Hegger R, Kantz H, and Schreiber T, Practical implementation of non-linear time series methods: The TISEAN package. CHAOS 9 (1999) 413–435.

[20] Kantz H, Schreiber T, Non-linear Time Series Analysis, Cambridge University Press, Cambridge, 1997.

[21] Abarbanel, H.D.I. Analysis of Observed Chaotic Data, Springer, Berlin, 1996.

[22] A.M. Fraser and H.L. Swinney, Independent coordinates for strange attractors from mutual information, Phys. Rev. A 33 (1986) 1134–1140.

[23] J.-P. Eckmann, S.O. Kamphorst, and D. Ruelle, Recurrence plots of dynamical systems, Europhys. Lett. 5 (1987) 973–977.

[24] C.L. Webber, Jr., and J.P. Zbilut, Dynamical assessment of physiological systems and states using recurrence plot strategies, J. App. Physiol. 76, (1994) 965–973.

[25] N. Marwan, Encounters with Neighbours: Current Development of Concepts Based on Recurrence Plots and their Applications, PhD Thesis, Universität Potsdam, Potsdam 2003.

[26] N. Marwan, Recurrence Plots Code, http:// www.agnld.uni- potsdam.de/ ∼marwan/6.download/rp.php (2006).

[27] M.B. Kennel, R. Brown, H.D.I. Abarbanel, Determining embedding dimension for phase-space reconstruction using a geometrical construction, Physical Review A 45 (1992) 3403–3411.

[28] Casdagli, M.C., Recurrence plots revisited, Physica D 108 (1997) 12–44.

[29] N. Marwan, M. C. Romano, M. Thiel and J. Kurths, Recurrence plots for the analysis of complex systems, Physics Reports 438 (2007) 237–329.

[30] G. Litak, A. Syta, and R. Rusinek, Dynamical changes during composite milling: recurrence and multiscale entropy analysis, Int. J. Adv. Man. Tech. 56 (2011) 445–453

[31] G. Litak, A. Syta, J. Gajewski, and J. Jonak, Detecting and identifying non-stationary courses in the ripping head power consumption by recurrence plots, Meccanica 45 (2010) 603–608.